



cluding crystals of nanocrystals, in which the spacing between crystallites can be altered at will, and quantum dot molecules, in which dots of several different materials and sizes are linked together. New physics and chemistry are sure to be discovered as these complex assemblies are investigated.

## REFERENCES AND NOTES

1. L. E. Brus, *Appl. Phys. A* **53**, 465 (1991).
2. T. Vossmeier, L. Katsikas, M. Giersig, I. G. Popovic, H. Weller, *J. Phys. Chem.* **98**, 7665 (1994).
3. V. L. Colvin, A. P. Alivisatos, J. G. Tobin, *Phys. Rev. Lett.* **66**, 2786 (1991).
4. A. N. Goldstein, C. M. Echer, A. P. Alivisatos, *Science* **256**, 1425 (1992).
5. S. H. Tolbert, and A. P. Alivisatos, *Annu. Rev. Phys. Chem.* **46**, 595 (1995).
6. V. L. Colvin, M. C. Schlamp, A. P. Alivisatos, *Nature* **370**, 354 (1994).
7. B. O. Dabbousi, M. G. Bawendi, O. Onitsuka, M. F. Rubner, *Appl. Phys. Lett.* **66**, 1316 (1995).
8. M. L. Cohen, M. Y. Chou, W. D. Knight, W. A. de Heer, *J. Phys. Chem.* **91**, 3141 (1987); C. Ellert, M. Schmidt, C. Schmitt, T. Reiners, H. Haberland, *Phys. Rev. Lett.* **75**, 1731 (1995).
9. A. Liu, Q.-L. Zhang, F. K. Tittel, R. F. Curl, R. E. Smalley, *J. Chem. Phys.* **85**, 7434 (1986).
10. M. Grundemann *et al.*, *Phys. Rev. Lett.* **74**, 4043 (1995).
11. C. B. Murray, C. R. Kagan, M. G. Bawendi, *Science* **270**, 1335 (1995).
12. C. B. Murray, D. J. Norris, M. G. Bawendi, *J. Am. Chem. Soc.* **115**, 8706 (1993).
13. S. Schmitt-Rink, D. A. B. Miller, D. S. Chemla, *Phys. Rev. B* **35**, 8113 (1987).
14. A. P. Alivisatos *et al.*, *J. Chem. Phys.* **89**, 4001 (1988).
15. R. W. Schoenlein, D. M. Mittleman, J. J. Shiang, A. P. Alivisatos, C. V. Shank, *Phys. Rev. Lett.* **70**, 1014 (1993).
16. W. E. Moerner, *Science* **265**, 46 (1994).
17. J. K. Trautman, J. J. Macklin, L. E. Brus, E. Betzig, *Nature* **369**, 40 (1994).
18. A. Mews, A. Eychmüller, M. Giersig, D. Schooss, H. Weller, *J. Phys. Chem.* **98**, 934 (1994).
19. L. T. Canham, *Appl. Phys. Lett.* **57**, 1064 (1990).
20. L. E. Brus *et al.*, *J. Am. Chem. Soc.* **117**, 2915 (1995).
21. S. H. Tolbert, A. B. Herhold, C. S. Johnson, A. P. Alivisatos, *Phys. Rev. Lett.* **73**, 3266 (1994).
22. M. A. Kastner, *Rev. Mod. Phys.* **64**, 489 (1992).
23. F. R. Waugh *et al.*, *Phys. Rev. Lett.* **75**, 705 (1995).
24. X. Peng, T. Wilson, P. G. Schultz, A. P. Alivisatos, in preparation.
25. O. I. Micic *et al.*, *J. Phys. Chem.* **99**, 7754 (1995).
26. J. R. Heath, J. J. Shiang, A. P. Alivisatos, *J. Chem. Phys.* **101**, 1067 (1994).
27. W. Chen, J. M. Rehm, C. Meyers, M. I. Freedhof, G. McLendon, *Mol. Cryst. Liq. Cryst.* **252**, 79 (1994).
28. J. Lin, E. Cates, P. A. Bianconi, *J. Am. Chem. Soc.* **116**, 4738 (1994).
29. N. Herron, J. C. Calabrese, W. E. Farneth, Y. Wang, *Science* **259**, 1426 (1993).
30. Structural and optical characterization of this structure is described by A. Mews, A. V. Kadavanich, U. Banin, and A. P. Alivisatos (in preparation).
31. I would like to thank A. Mews, A. Kadavanich, and U. Banin for their assistance in the preparation of the manuscript.

# Magnetic Clusters in Molecular Beams, Metals, and Semiconductors

Jing Shi, S. Gider, K. Babcock, D. D. Awschalom\*

The evolution of magnetic order from the microscopic to the macroscopic regime may be studied with the use of nanometer-scale clusters. A variety of new techniques can be employed to control the size of the magnetic clusters from the atomic level. Molecular beams are used to construct and measure the magnetic properties of isolated metallic clusters. Superparamagnetic metallic particles embedded in a metal exhibit dramatic field-dependent changes in electrical conduction, providing a measure of spin-dependent scattering. Related efforts in semiconductor hosts with the use of ion implantation have generated room-temperature ferromagnetic clusters that can be directly imaged by magnetic force microscopy.

The magnetic properties of isolated atoms are well understood, but the development of magnetic order on a macroscopic scale in a crystal is a more formidable problem. Long-range magnetic order is not simply a superposition of the effects of individual atoms; it is a collective effect of atoms communicating through the Coulomb interaction and the Pauli exclusion principle. These exchange interactions may lead to an alignment (ferromagnetism), an alternation (antiferromagnetism), or more complicated arrangements of the magnetic moments. Magnetic clusters provide a link between magnetism on the microscopic atomic level and the macroscopic state; and by allowing us to observe magnetic order as it develops from individual magnetic atoms to large

crystals, such clusters can contribute to our understanding of magnetism in both regimes. Like the study of mesoscopic electronics (1), which may lead to more highly integrated circuits, mesoscopic magnetism is not only of academic interest but also of technological importance as magnetic recording densities continue to increase, requiring smaller bits to store information (2). In addition to information storage, magnetic clusters are being examined for diverse applications ranging from enhanced magnetic resonance images (3) to magnetic refrigeration (4).

A great deal of work on small magnetic particles and molecules exists (5). Here we describe a select set of recent developments aimed at construction and measurement of such systems in a wide variety of environments. The ideal experiment for the study of clusters would control their size with atomic precision and probe the properties of an isolated individual cluster instead of averaging over an ensemble. A close realization

of this ideal is the work on clusters formed in molecular beams, which are also advantageous because there is no interaction between clusters or with a surrounding medium. However, practical applications of magnetic clusters typically require a host. Magnetic clusters may be used to affect electron conduction or optical properties of their host, and in turn the host may have an effect on the magnetic properties of the clusters. In metals, magnetic clusters can produce an unusually large dependence of the resistance on magnetic field, an effect known as "giant magnetoresistance" (GMR) and originally observed in magnetic multilayers (6). The change in resistance upon application of a magnetic field is as high as ~20% for Co clusters in Ag and ~50% in the Fe/Cr multilayers, which is a large change when compared with the ~1% effect that is typical in bulk magnetic metals such as iron or nickel. Magnetoresistive materials are being pursued as a promising technology for the next generation of magnetic sensors and recording read heads. The incorporation of magnetic clusters in semiconductors would allow for the integration of microelectronics with recording and storage technologies, as well as enabling spin-dependent switching. Epitaxial growth techniques using semiconductors have been remarkably successful in providing layers of near-atomic thickness for electronic and optoelectronic devices (1), and have included recent success in interleaving of semiconductor and magnetic multilayers (7). Moreover, the dilution of magnetic atoms into a semiconductor heterostructure gives rise to a variety of new phenomena that are strongly sensitive to magnetic fields (8). However, there are a number of technological obstacles preventing the fabrication of practical devices; most suitable magnetic ions tend to order antiferromagnetically and only at low temperatures, generating no net magnetic moment (8).

J. Shi, S. Gider, and D. D. Awschalom are in the Department of Physics, University of California, Santa Barbara, CA 93106, USA. K. Babcock is with Digital Instruments, Santa Barbara, CA 93103, USA.

\*To whom correspondence should be addressed.

Progress toward overcoming these difficulties has recently been made by the introduction of magnetic ions ( $\text{Mn}^{2+}$ ) into a semiconductor (GaAs) by implantation and subsequent annealing to form room-temperature ferromagnetic clusters of a new compound, GaMn. Advances in magnetic force microscopy have enabled the direct observation of the magnetic field dependence and switching of individual clusters.

The majority of the work reviewed here is experimental, but magnetic clusters are also the subject of substantial theoretical work, in part because theoretical models of clusters are more amenable to exact calculations (9). One of the most intriguing prospects is the use of magnetic moments for computational logic as well as memory (10).

### Free Clusters in Molecular Beams

Molecular beams provide atomic control of the size of clusters of various elements, including transition metals and rare earths, elucidating the evolution of magnetic order from the atomic to the bulk level without the complication of a host. Atoms of transition metals and rare earths are generally paramagnetic, possessing a moment that can be aligned to a field but no remanent moment after removal of the field. A few of these elements are ferromagnetic when crystallized, acquiring a permanent magnetic moment; however, the magnetic moment per atom is not necessarily the same in the paramagnetic and ferromagnetic states. For example, an iron atom has a paramagnetic moment as large as  $6 \mu_B$  ( $\mu_B$  is the Bohr magneton, the magnetic moment of an electron), but a bulk crystal of body-centered-cubic (bcc) iron below the temperature  $T = 1043 \text{ K}$  is ferromagnetic with an average moment per atom of  $2.22 \mu_B$ . The loss of moment and the appearance of an average nonintegral moment are characteristic of the transition metal ferromagnets (iron, cobalt, and nickel). This is related to exchange interactions between  $3d$  electrons in delocalized states, or bands, and is known as itinerant exchange (11, p. 300). The change in magnetic character from atomic to itinerant may be studied with clusters in molecular beams. Furthermore, because magnetism in transition metals is closely tied to the electronic band structure, and in turn to the crystal structure, different types of magnetic order may emerge because clusters do not necessarily have the same crystal structure as does the bulk crystal.

The experiments on free clusters are descendants of the classic work in which the magnetic moment of the electron was first measured by Otto Stern and Walter Gerlach 70 years ago. Unlike the atoms used in the Stern-Gerlach experiment, however, clusters cannot be formed contin-

uously by evaporation but must instead be formed by a pulsed technique. A pulsed laser vaporizes a target material, and the metal vapor is then rapidly quenched by a high-pressure helium gas jet ( $\sim 7 \times 10^3$  torr). From the relatively high-pressure source chamber, the clusters and helium gas expand into a low-pressure ( $\sim 10^{-7}$  torr) collimation chamber to produce a supersonic beam. The beam is then directed toward a gradient magnet, which deflects the clusters according to the projection of their magnetic moment on the gradient field direction. Finally, the beam intensity of each cluster size is profiled by a time-of-flight mass spectrometer.

The first dramatic observation concerning free magnetic clusters was that the beam only deflects in one direction (12), unlike the situation in the original Stern-Gerlach experiment, in which the beam of silver atoms was divided equally. The magnetic moment of a silver atom is proportional to the spin angular momentum  $S$ . Without collisions between atoms (which are rare in molecular beams) and without contact with any other energy reservoir, the magnetic states  $S = +\frac{1}{2}$  and  $S = -\frac{1}{2}$  will be equally populated, even in the presence of a uniform field superimposed on the gradient field. The gradient field in the Stern-Gerlach experiment will therefore separate the beam into two symmetric peaks. However, clusters of atoms have additional degrees of freedom such as rotation of the cluster as a whole, with which the magnetic states may exchange angular momentum. Energy conservation is affected by further interactions with the vibrations. The magnetic states of a cluster will not be equally populated, eventually equilibrating toward a Boltzmann distribution, which in the presence of a uniform field would align the average magnetic moment with the field. The gradient field thereby deflects the beam of clusters in only one direction.

A homogenous deflection in only one direction further implies that the magnetic moment is dynamically decoupled from the lattice, with anisotropy barriers which are small as compared with thermal energies. The magnetic moments are locked together by exchange interactions; hence, the moments rotate in unison with respect to the lattice. The cluster thus behaves like a paramagnet but with a much larger net moment than that of a single paramagnetic atom, that is, a "superparamagnet." Superparamagnetism is a well-known phenomenon in small magnetic particles (11, p. 360) and was proposed for clusters to explain the observation of lower magnetization value per atom than that of the bulk for  $3d$ -series transition metals (13). When the magnetization is understood as the time averaged projection of a superparamagnetic moment,

the magnitude of the moment is found to be larger than that of the bulk for  $3d$  transition metals. As is in agreement with the theory of superparamagnetism, the average deflection is proportional to the magnetic field strength and the square of the moment and is inversely proportional to the temperature. The temperature of the clusters is taken as the temperature of the source: For long times in the source, clusters will suffer more collisions with the carrier gas and will eventually equilibrate with the source temperature. As the source temperature is lowered, there is not enough thermal energy available for the magnetization to overcome the crystalline field anisotropy energy barrier. This blocking of the magnetization is manifest in small particles by the appearance of hysteresis and in clusters in molecular beams by an inhomogeneous broadening of the beam (14), reflecting the inability of the clusters to thermalize and align with the field (Fig. 1).

In the superparamagnetic regime, the magnitude of the average moment per atom can also be studied as a function of the cluster size. As the size of clusters of transition metals such as Fe, Co, and Ni increases, the moment per atom should decrease as the character of the moments changes from atomic to itinerant. Experiments have shown that the moment does decrease and eventually reaches the bulk limit for clusters around 500 atoms (Fig. 2A) (15, 16). The decrease is not entirely monotonic and appears to be oscillatory, suggesting a finite size effect. Experiments suggest that Co and Ni clusters may form as icosahedra (17). Perfect icosahedra occur for clusters with 13, 55, 147, 309, and 561 atoms and correspond to 1 through 5 completed shells of atoms. It can be argued that clusters with these numbers of atoms should have reduced magnetic moment values as com-

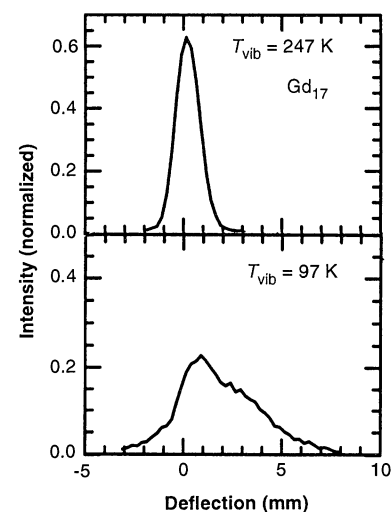
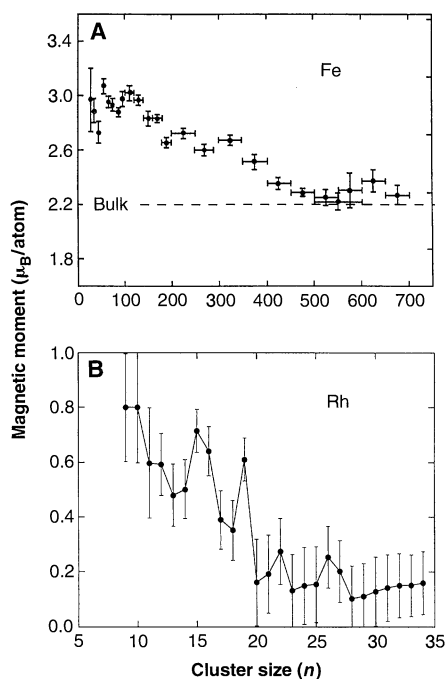


Fig. 1. Beam profiles for  $\text{Gd}_{17}$  clusters at lower temperatures [from (14)].

pared with open-shell clusters, as for example in  $\text{Ni}_{13}$  and  $\text{Ni}_{55}$  (18). Another study (16) finds that the extrema of the oscillations are not solely related to geometric effects, suggesting that electronic effects are probably as important in these itinerant magnetic systems. Studies of other transition metals and rare earths have also produced interesting results. Rhodium, which is not magnetic in bulk form, has been observed to form magnetic clusters (Fig. 2B); however, ruthenium and palladium, which are beside rhodium in the 4d series, are not magnetic, even in clusters (19).

### Magnetic Clusters in Metals

The study of free clusters is important in understanding the development of magnetic order from the atomic level; however, such clusters are not stable outside the molecular beam chamber. For example, free clusters are susceptible to oxidation and aggregation. One method by which to render clusters stable is to surround them with a protein shell as in the biological magnet ferritin or with organic ligands as in molecular magnets (5). A more commonly used method is to embed them in a solid host. Giant magnetoresistive granular materials (20, 21) represent an important class of magnetic nanostructures in metallic systems that exemplify how reduced length scales affect both magnetic and electron transport properties (22). Originally, GMR was observed in multilayers consisting of alternating magnetic and nonmagnetic materials



**Fig. 2.** The magnetic moment per atom as a function of cluster size for (A) Fe [from (15)] and (B) Rh [from (19)].

(6). The GMR effect in multilayers is very sensitive to the thickness and spacing of the layers, requiring control of layer growth with atomic monolayer precision. The observation of GMR in granular materials, which do not require nearly the same degree of control, was therefore quite unexpected.

In a metallic system, small particle sizes (a few nanometers) and a wide range of interparticle spacings can be readily realized. Among a number of techniques, the one most commonly used for producing such microscopic granular samples takes advantage of the phase separation of metastable alloys, which consist of two immiscible metals. These metallic constituents may be elemental metals (for example, Fe, Co, Cu, and Ag), crystalline alloys (for example, Fe-Ni), metastable crystalline alloys (for example, Fe-Cu), or amorphous alloys (for example, Fe-BN) (22). Although these particles are much larger than the clusters in molecular beams, consisting of  $10^3$  to  $10^6$  atoms, and therefore have a larger crystalline anisotropy energy barrier, they still display superparamagnetism at and below room temperature. However, to electrons traveling at the Fermi velocity, the superparamagnetic moments are effectively blocked; therefore, the fluctuations during the time scale of the magnetization measurement ( $\sim 100$  s) do not affect the electron transport because the electrons sample the moments on a faster time scale ( $\sim 10^{-9}$  s). Even at temperatures at which the magnetization does not show any remanent moment, the GMR effect is still observed. The electronic structure of the metallic host does not appear to have a substantial effect

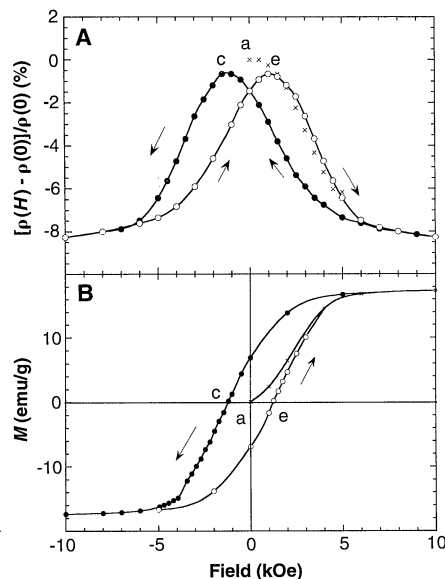


**Fig. 3.** (A) Magnetoresistance and (B) hysteresis loop of the same  $\text{Co}_{46}\text{Cu}_{54}$  granular sample (annealed at  $350^\circ\text{C}$ ) at  $T = 5$  K [from (22)]. The crosses denote the initial curves.

on the magnetic particles because similar magnetic properties are observed for particles embedded in an insulating host (22).

If an electron in the metal is successively scattered by magnetic granules before it flips its spin, the relative orientation of magnetic moments of these granules affects the spin-dependent scattering rate. When an external magnetic field changes the orientation of the moments, the scattering rate also changes, thus causing the resistance to depend on the applied magnetic field strength (Fig. 3). In granular systems, the separation  $l$  between the magnetic clusters can be varied by control of the volume fraction and the growth of granules. If  $l$  is much larger than electron mean-free-path, many intermediate scattering events randomize the spin information of electrons. Thus, the scattering rate is independent of magnetization and there is no GMR; alternatively, if  $l$  is so short that an infinite percolation network is developed due to the exchange interaction between magnetic granules, then the GMR effect vanishes. In a Co-Ag sample (22), for example, a volume content of Co between 15 and 40% gives a sizable magnetoresistance effect (Fig. 4A). In a GMR system, each individual granule moment contributes to spin-dependent scattering, and the magnetoresistance is directly related to the global magnetization  $M$ . In fact, the magnetoresistance is a

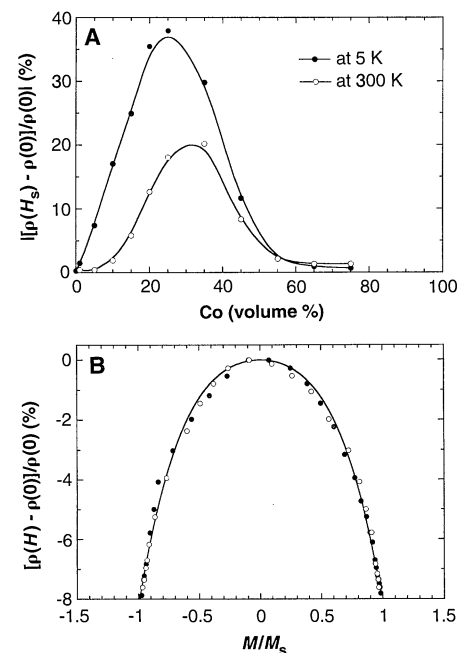


**Fig. 4.** (A) Magnetoresistance ratio  $|\rho(H_s) - \rho(0)|/\rho(0)$  of Co-Ag as a function of Co content in volume % at  $T = 5$  K and 300 K. (B) Magnetoresistance versus normalized magnetization  $M/M_s$ . Both resistance and magnetization data in this plot are the data shown in Fig. 3, and the solid line is a fit to  $M^2$  dependence with an  $M^4$  correction term [from (22)].

function of  $(M/M_s)^2$ , where  $M_s$  is the saturation magnetization (21). A distribution of particle sizes (23) or interparticle correlation (24) can lead to a higher order correction to a simple quadratic dependence (Fig. 4B).

The GMR effect that occurs in granular solids can be described by a two-current model, just as in multilayer structures. In the two-current model language, spin-dependent scattering is equally effective for both spin-up and -down electrons in a disordered state, whereas in an ordered state with the granule moments aligned in the field direction, one spin channel is less resistive than the other because of the asymmetry between them. The less resistive channel therefore shorts out the current conduction and the resistance drops in an applied field (23). This reduction in the electrical resistance can be as high as 20% at room temperature. Moreover, the change in the resistance,  $\Delta\rho$ , is correlated with the radius  $r$  of the magnetic granules (21) ( $\Delta\rho \sim 1/r$ ). The fact that the change in the resistance is directly proportional to the ratio of the area of interfaces to the volume of the magnetic granules suggests that the spin-dependent scattering occurs only at the interfaces between the granules and the matrix. The same spin-dependent scattering also produces giant magnetothermoelectric power (25) and magnetothermal conductivity (26).

### Magnetic Nanostructures in Semiconductors

Microscopic ferromagnets can be fabricated on semiconductor substrates in a number of ways, including electron-beam lithographic patterning (27), scanning tunneling microscope deposition (28), and electrochemical etching and electrodeposition (29). In order to enhance the effective interaction between electronic carriers and local ferromagnetic fields, it is desirable to locate ferromagnetic clusters within a semiconductor. This is a challenge because the solubility of magnetic ions in semiconductors is generally low. Because Mn ions replace Ga in the GaAs lattice and act as acceptors, it is possible to incorporate localized ferromagnetic structures inside the GaAs semiconductor while preserving its electronic and optical properties. This may be achieved by ion implantation and subsequent heat treatment (30, 31). Although the solubility of Mn ions in GaAs is very low under equilibrium conditions, a relatively high concentration ( $\sim 10^{21} \text{ cm}^{-3}$ ) can be obtained by implantation of the ions into the semiconductor. During rapid thermal annealing at  $T > 600^\circ\text{C}$ , the uniformly implanted Mn ions diffuse and combine with Ga to form submicron GaMn microcrystallites (150 to 400 nm in diameter), which are ferromagnetic at room tempera-

ture. A structure containing an ensemble of particles has a magnetization that can be reversed at the coercive field  $H_c \sim 6 \text{ kOe}$  and becomes paramagnetic above the Curie temperature  $T_c > 400 \text{ K}$ . These particles are larger than the typical magnetic particles (1 to 10 nm in diameter) in granular GMR materials and, in fact, are large enough that the magnetic moments may not be uniform throughout the particle; that is, the particle consists of magnetic domains. In this instance, the GaAs host plays an important role in determining magnetic properties such as the domain orientation.

The GaMn ferromagnets are formed near the GaAs surface and may be directly probed by atomic (AFM) and magnetic force microscopy (MFM) at room temperature (31, 32). In MFM images (Fig. 5), the contrast is caused by spatial variations in the magnetic interaction between the magnetized probe and the stray magnetic fields of the sample. Although the ferromagnetic

particles ( $\sim 400 \text{ nm}$  in diameter) produce strong magnetic force contrast, there exist particles ( $\sim 50\%$ ) that show only weak contrast. The latter particles are likely to be ferromagnets with very low coercive fields and moment densities or possibly even superparamagnets at room temperature (33).

One can infer the magnetic state of the GaMn precipitates from these MFM images. To a good approximation, the MFM probe behaves like a localized magnetic dipole (32), and the imaging of spherical single-domain particles can be modeled by a dipole-dipole interaction. Figure 6 shows calculated single-particle images based on this approximation for four different configurations. A more detailed model that integrates dipole moments over the surface of the tip produces similar node structures. These simulations show that one can obtain a variety of patterns from a single-domain particle, depending on the relative orientation between the tip and particle moments. However, with a perpendicularly magnetized tip such as was used to produce the data in Fig. 5, the simulations of single-domain particles do not show the complicated four-component contrast observed (Fig. 5A). Thus, these two precipitates must be multidomain magnetic particles, whereas the others are single-domain particles. Figures 6C and 6D are characteristic of MFM

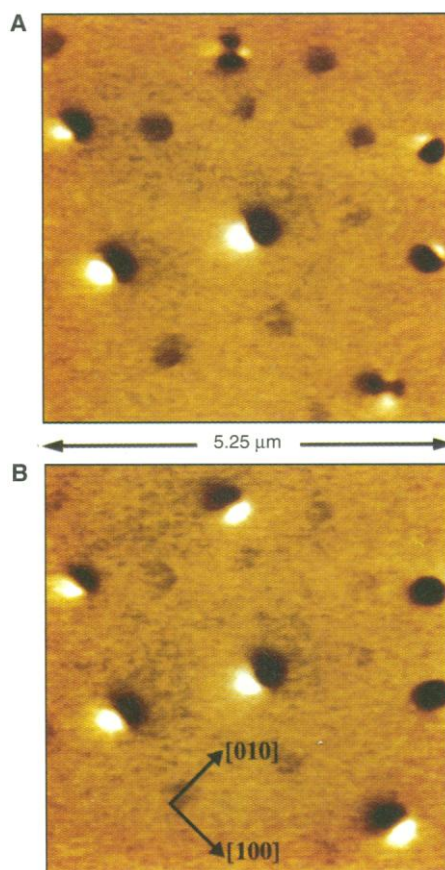


**Fig. 5.** Magnetic force images of an implanted ( $10^{15} \text{ Mn}^+ \text{ cm}^{-2}$ ) and annealed (at  $920^\circ\text{C}$  for 60 s) sample before (A) and after (B) it was magnetized with a perpendicular magnetic field ( $\sim 2 \text{ kOe}$ ). Upon application of the magnetizing field, multidomain particles that show four-component patterns in (A) are converted to single-domain particles in (B), and moments preferentially align with  $\langle 100 \rangle$ ,  $\langle 010 \rangle$ ,  $\langle 001 \rangle$  directions of the GaAs substrate. The Co-Cr-coated MFM tip was magnetized perpendicular to the sample surface.

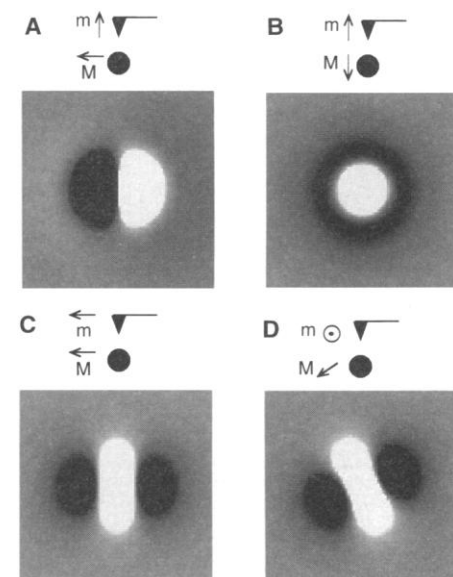


**Fig. 6.** Simulations of magnetic force images of a single-domain particle. (A) and (B) correspond to particles whose moment ( $M$ ) is parallel and perpendicular to the surface plane, respectively, and imaged with a tip whose moment ( $m$ ) is perpendicular to the surface plane. A perpendicular particle moment with an in-plane tip moment produces the same pattern as in (A). (C) corresponds to an in-plane moment and a tip magnetized parallel to the particle moment, and (D) corresponds to an in-plane moment and tip magnetized parallel to the surface but at  $45^\circ$  to the moment.



images captured in the presence of a strong in-plane magnetic field, where the tip is forced to align with the field. Such simulations demonstrate the importance of understanding the interplay between instrumental sensor and sample cluster magnetic fields for meaningful particle imaging in mesoscopic dimensions.

In an unmagnetized sample, particles within this length scale can be single-domain or multidomain. Upon application and removal of a perpendicular magnetic field ( $\sim 2$  kOe) to an unmagnetized sample, multidomain GaMn particles are converted to single-domain particles (Fig. 5B); in particular, the single-domain moments are observed to preferentially align along the three equivalent crystalline axes ( $\langle 100 \rangle$ ,  $\langle 010 \rangle$ ,  $\langle 001 \rangle$ ) of the GaAs host after the field is removed (31). The behavior of ferromagnetic particles can also be studied by continuous application of an in-plane field (33). For fields stronger than the tip coercive field ( $\sim 400$  Oe), the tip is forced to align with the in-plane field, thus allowing simple image interpretation. As the in-plane field is increased, the moments tend to align with the field direction, displaying two types of motion: discontinuous reversal and gradual rotation of the magnetization, depending on the relative orientation between the magnetic easy axis and the applied field.

These processes can be investigated directly by imaging single particles in real time while ramping the in-plane applied field. Figure 7 shows two extreme cases: one with the easy axis parallel and the other perpendicular to the field direction. A complete reversal is clearly seen in the left-hand image and the corresponding switching field is  $\sim 4$  kOe. In the right-hand image, the perpendicular moment undergoes a gradual rotation from its initial orientation, toward a partial alignment with the field. The field required to fully align the moment is estimated to be  $\sim 7.5$  kOe. This field would be equal to the switching field for the parallel moment ( $\sim 4$  kOe), if the two particles were identical (11, p. 344). A large variation (about a factor of 3) in the switching field is also found among

particles with approximately the same easy axis orientation. As these particles are likely to have the same crystalline structure with similar strain, this variation may be due to shape anisotropy. Further investigations should reveal the magnetic anisotropy and micromagnetic behavior of these single-domain magnets as well as their role in modifying electronic transport.

## Conclusions

There are increasingly varied ways to fabricate and examine magnetic clusters down to atomic length scales without and within different host materials. The study of free magnetic clusters in the absence of a host is only beginning. The dynamics of the magnetization are likely to change dramatically as the temperature is lowered, and it is possible that exotic phenomena such as macroscopic quantum tunneling of the magnetization will be revealed (5). The intrinsic behavior of clusters can affect host properties such as electron transport in metals, and the host may in turn strongly influence cluster properties such as the domain orientation in semiconductors. Although current granular GMR materials do not have a strong enough field sensitivity to be practical for magnetic recording, they may nevertheless be useful where Hall bar position and motion sensors are currently used, such as in automobile timing circuits and videocassette recorders. The effect of magnetic clusters on electron transport in semiconductors is a nascent area rich in possibilities for exploration. In addition to the many scientific issues, there is a strong technological drive to develop ultrafast spin-dependent electronics, integrated magneto-optics, and high-density magnetic storage. These areas of research demonstrate that advances in understanding of mesoscopic magnetism are concomitant with advances in novel experimental techniques. For example, the force detection of nuclear magnetic resonance (34) has the theoretical capability of allowing identification of atomic spe-

cies in a molecule with spatial resolution. Although one motivation for studying nanometer-scale clusters was to simplify an otherwise complicated macroscopic system, the magnetic properties of clusters have proved to be surprisingly complex.

## REFERENCES AND NOTES

1. F. Capasso, *Phys. Today* **43** (no. 2), 22 (1990).
2. J. L. Simonds, *ibid.* **48** (no. 4), 26 (1995).
3. J. W. M. Bulte *et al.*, *J. Magn. Reson. Imag.* **4**, 497 (1994).
4. R. D. Shull, R. D. McMichael, J. J. Ritter, *Nanostruct. Mat.* **2**, 205 (1993).
5. For a review, see D. D. Awschalom and D. P. DiVincenzo, *Phys. Today* **48** (no. 4), 43 (1995).
6. For a review, see A. Barthélemy, A. Fert, R. Morel, L. Steren, *Phys. World* **7**, 34 (1994).
7. M. Tanaka *et al.*, *Solid-State Electron.* **37**, 1031 (1994).
8. J. K. Furdyna and J. Kossut, Eds., *Semiconductors and Semimetals*, vol. 25, *Diluted Magnetic Semiconductors* (Academic Press, San Diego, CA, 1988).
9. D. Garcia-Pablos, P. A. Serena, N. Garcia, H. D. Raedt, *Phys. Rev. B*, in press; G. Levine and J. Howard, *Phys. Rev. Lett.* **75**, 4142 (1995).
10. D. P. DiVincenzo, *Science* **270**, 255 (1995).
11. A. H. Morrish, *The Physical Principles of Magnetism* (Wiley, New York, 1965).
12. W. A. de Heer, P. Milani, A. Châtelain, *Phys. Rev. Lett.* **65**, 488 (1990); J. P. Bucher, D. C. Douglass, L. A. Bloomfield, *ibid.* **66**, 3052 (1991).
13. S. N. Khanna and S. Linderoth, *ibid.* **67**, 742 (1991); P. J. Jensen, S. Mukherjee, K. H. Bennemann, *Z. Phys. D* **21**, 349 (1991).
14. D. C. Douglass, A. J. Cox, J. P. Bucher, L. A. Bloomfield, *Phys. Rev. B* **47**, 12874 (1993).
15. I. M. L. Billas, J. A. Becker, A. Châtelain, W. A. de Heer, *Phys. Rev. Lett.* **71**, 4067 (1993).
16. I. M. L. Billas, A. Châtelain, W. A. de Heer, *Science* **265**, 1682 (1994).
17. E. K. Parks, B. J. Winter, T. D. Klots, S. J. Riley, *J. Chem. Phys.* **94**, 1882 (1991); M. Pellarin *et al.*, *Chem. Phys. Lett.* **217**, 349 (1994).
18. S. E. Apsel, J. W. Emmert, J. Deng, L. A. Bloomfield, in preparation.
19. A. J. Cox, J. G. Louderback, S. E. Apsel, L. A. Bloomfield, *Phys. Rev. B* **49**, 12295 (1994).
20. A. E. Berkowitz *et al.*, *Phys. Rev. Lett.* **68**, 3745 (1992).
21. J. Q. Xiao, J. S. Jiang, C. L. Chien, *ibid.*, p. 3749.
22. For a review, see C. L. Chien, *Annu. Rev. Mat. Sci.* **25**, 129 (1995).
23. S. Zhang and P. M. Levy, *J. Appl. Phys.* **73**, 5315 (1993).
24. C. L. Chien, J. Q. Xiao, J. S. Jiang, *ibid.*, p. 5309.
25. J. Shi, E. Kita, L. Xing, M. B. Salamon, *Phys. Rev. B* **48**, 16119 (1993).
26. L. Piroux *et al.*, *J. Magn. Magn. Mat.* **136**, 221 (1994); J. Shi, K. Pettit, E. Kita, S. S. P. Parkin, M. B. Salamon, *Phys. Rev. B*, in press.
27. J. F. Smyth *et al.*, *J. Appl. Phys.* **69**, 5262 (1991); M. S. Wei and S. Y. Chou, *ibid.* **76**, 6679 (1994); R. M. H. New, R. F. W. Pease, R. L. White, *J. Vac. Sci. Technol. B* **13**, 1089 (1995).
28. A. D. Kent, T. M. Shaw, S. von Molnár, D. D. Awschalom, *Science* **262**, 1249 (1993).
29. S. A. Gusev, N. A. Korotkova, D. B. Rozenstein, A. A. Fraerman, *J. Appl. Phys.* **76**, 1994 (1994).
30. J. Shi *et al.*, *Nature* **377**, 707 (1995).
31. J. Shi, J. M. Kikkawa, D. D. Awschalom, P. M. Petroff, K. Babcock, *J. Appl. Phys.*, in press.
32. K. Babcock, M. Dugas, S. Manalis, V. Elings, *Mat. Res. Soc. Symp. Proc.* **355**, 311 (1995).
33. R. D. Gomez, I. D. Mayergoyz, E. R. Burke, *IEEE Trans. Magn.* **331**, 3346 (1995).
34. D. Rugar *et al.*, *Science* **264**, 1560 (1994).
35. We thank L. A. Bloomfield, C. L. Chien, W. A. de Heer, J. S. Jiang, and J. Q. Xiao for their help with the manuscript. Parts of this work were supported by grants from the Air Force Office of Scientific Research (F49620-93-1-0117), the NSF Center for Quantized Electronic Structures (DMR-91-20007), and the NSF Materials Research Laboratory (DMR-9123048).

**Fig. 7.** Images of dipolar moments (M) with increasing in-plane magnetic field. The MFM tip repeatedly scanned over the middle of each 400-nm particle. The left (right) particle has its easy axis parallel (perpendicular) to the field direction. The symbols shown to the left and right of the MFM images represent the corresponding whole-particle images (similar to those shown in Fig. 6, A, C, and D) at different fields.

